Interspecific scaling of blood flow rates and arterial sizes in mammals

Roger S. Seymour[1]*, Qiaohui Hu[1], Edward P. Snelling[2,3] and Craig R. White[4]

[1]*School of Biological Sciences, Faculty of Sciences, University of Adelaide, Adelaide, South Australia 5005, Australia*

[2]*Department of Anatomy and Physiology, Faculty of Veterinary Science, University of Pretoria, Onderstepoort, Gauteng 0110, South Africa*

[3]*Brain Function Research Group, School of Physiology, Faculty of Health Sciences, University of the Witwatersrand, Johannesburg, Gauteng 2193, South Africa*

[4]*Centre for Geometric Biology, School of Biological Sciences, Faculty of Science, Monash University, Clayton, Victoria 3800, Australia*

Orcid ID: R.S.S., 0000-0002-3395-0059; Q.H., 0000-0003-3163-7859; E.P.S., 0000-0002-8985-8737; C.R.W., 0000-0002-0200-2187

*Author for correspondence e-mail: roger.seymour@adelaide.edu.au

         Phone: +61 8 8313 5596

Summary statement: Blood flow rate along arteries is analysed in relation to arterial size, body mass and basal metabolic rate in mammals at rest.

ABSTRACT

This meta-study investigates the relationships between blood flow rate ($\dot{Q}$; cm^3 s^{-1}), wall shear stress (τ; dyne cm^{-2}) and lumen radius (r_i; cm) in 20 named systemic arteries of nine species of mammals, weighing from 23 g mice to 652 kg cows, at rest. In the dataset, derived from 50 studies, lumen radius varies between 3.7 μm in a cremaster artery of a rat to 11.2 mm in the aorta of a human. The 92 logged data points of $\dot{Q}$ and r_i are described by a single second-order polynomial curve with the equation, log $\dot{Q}$ = -0.20 log r_i^2 +1.91 log r_i + 1.82. The slope of the curve increases from approximately 2 in the largest arteries to approximately 3 in the smallest ones. Thus, da Vinci's Rule ($\dot{Q} \propto r_i^2$) applies to the main arteries and Murray's Law ($\dot{Q} \propto r_i^3$) applies to the microcirculation. A subset of the data, comprising only cephalic arteries in which $\dot{Q}$ is fairly constant, yielded the allometric power equation, $\dot{Q}$ = 155 $r_i^{2.49}$. These empirical equations allow calculation of resting perfusion rates from arterial lumen size alone, without reliance on theoretical models or assumptions on the scaling of wall shear stress in relation to body mass. As expected, $\dot{Q}$ of individual named arteries is strongly affected by body mass, however, $\dot{Q}$ of the common carotid artery from six species (mouse to horse) is also sensitive to differences in whole-body basal metabolic rate, independent of the effect of body mass.

KEY WORDS: Artery, Blood flow rate, Circulation, da Vinci's Rule, Murray's Law, Wall shear stress

List of abbreviations

η blood viscocity (dyne s cm^{-2})

τ wall shear stress (dyne cm^{-2})

BMR   basal metabolic rate (ml O$_2$ h^{-1})

M_b body mass (kg)

$\dot{Q}$ volume blood flow rate (cm^3 s^{-1})

r_i internal radius (cm)

INTRODUCTION

The systemic arteries of mammals carry oxygenated blood to the tissues to support their aerobic metabolic demands. Therefore, there is a functional link between the size of the arteries, the rate of blood flow they transmit, and the metabolic demand of the supplied tissues. Metabolic rate scales allometrically with body size, so there are likely to be patterns of cardiovascular variables that relate to body size in a functionally meaningful way. The empirical relationships between mammalian body size and heart mass, stroke volume, heart rate, cardiac output and blood pressure have each been shown to be related to metabolic rate, either directly or indirectly (Calder, 1996; Hillman and Hedrick, 2015; Seymour and Blaylock, 2000). The branching morphology of the arterial system has been measured and modelled to test the optimality theory of a space-filling fractal network that supplies oxygenated blood with the least energy cost (Brummer et al., 2017; Hunt and Savage, 2016; Huo and Kassab, 2012; Huo and Kassab, 2016; Kassab, 2006; Newberry et al., 2015; Price et al., 2007; Tekin et al., 2016). However, most of these studies focus only on the morphology of the network, and so it is difficult to extract the relationships between arterial sizes and actual blood flow rates. To address this limitation, the present study takes an empirical approach by searching the literature and collecting paired measurements of arterial lumen radii and blood flow rates in 20 named systemic arteries of mammals. We hypothesize that the sizes of branching arteries should be related to the rate of blood flow within them, which depends directly on the absolute metabolic demand of the tissues, and indirectly on body size.

Correlations between the metabolic rates of animals and the structure of supply networks are well known, but the direction of dependence is confusing in the literature. West, Brown and Enquist began a revolution in thinking about physiological scaling by suggesting that quarter-power scaling of metabolic rate and other traits should arise if vascular networks are selected to fill space while minimising the energy required to distribute resources (Brummer et al., 2017; West et al., 1997). The vascular system has therefore been hypothesised to determine rates of metabolism (Newberry et al., 2015). An alternative perspective is that the allometric scaling of metabolic rate arises for reasons unrelated to the geometry of the vascular system (Kozłowski and Weiner, 1997). The need to deliver oxygen and nutrients to fuel rates of metabolism would then determine the structure of the vascular system. Distinguishing between the evolutionary explanations for the origin of metabolic scaling is challenging, but there are numerous examples demonstrating that metabolic demand determines the structure of the circulatory system. For example, the number and size of arteries are dynamically and reversibly adjusted throughout life to match the required rates of blood flow. Arteriogenesis (the increase in arterial diameter and wall thickness) and angiogenesis (the increase in the number of vessels by splitting or sprouting) occur in response to increases in metabolic demand of

growing organs (Heil et al., 2006). The same phenomena occur in skeletal muscles during athletic training (Prior et al., 2004; Thijssen et al., 2012). Tumour metabolism becomes limited by perfusion during rapid growth, resulting in anaerobic metabolism and lactate that stimulates angiogenesis and subsequent oxygenation (Polet and Feron, 2013). Experimental changes in blood flow regime of major arteries result in appropriate changes in diameter and wall thickness (Caro et al., 2012; Kamiya et al., 1984; Kamiya and Togawa, 1980; Langille, 1999; Smiesko and Johnson, 1993; Tronc et al., 1996; Wolinsky and Glagov, 1967). The success of coronary bypass surgery in which a vein is substituted for the diseased artery is due to the fact that the vein assumes the morphology similar to that of a healthy artery in a matter of weeks (Owens, 2010). It is clear that the morphology of the arteries is responsive to changes in metabolic demand, through changes in blood flow rate and blood pressure.

The physiological mechanisms responsible for controlling arterial size involve reversible interactions between blood flowing adjacent to the endothelium of the vessels, and circumferential wall tension caused by blood pressure (Lu and Kassab, 2011). Higher blood flow rates over the glycocalyx of the endothelium initiate a series of responses involving inflammation, nitric oxide, vascular endothelial growth factor receptor proteins, metalloproteinases, cytokines and extracellular matrix proteins (Baeyens et al., 2015; Reitsma et al., 2007; Silvestre et al., 2013). The result is cellular proliferation in the vessel wall that enlarges the lumen and reduces blood velocity near the wall (Lehoux et al., 2006). Because the effects are reversible, they are thought to normalize wall shear stress (WSS), which is an indirect measure of the stress on the glycocalyx of the endothelium. WSS (τ, dyne cm^{-2}) can be measured directly as the derivative of the velocity gradient adjacent to the wall (Papaioannou and Stefanadis, 2005). WSS can also be calculated from blood flow rate ($\dot{Q}$, cm^3 s^{-1}), blood viscosity (η, dyne s cm^{-2}) and arterial lumen radius (r_i, cm) according to the Poiseuille 'shear stress equation', $\tau = (4\,\dot{Q}\,\eta)/(\pi\,r_i^3)$, assuming that the flow conforms to the Poiseuille regime of a Newtonian fluid in a straight cylinder where the velocity profile is parabolic (Lehoux and Tedgui, 2003). However, the quantitative connection between the level of WSS and the extent of vascular remodeling is obscure, because WSS is either measured by the velocity gradient far from the wall or it is calculated from the shear stress equation without reference to the wall at all. Thus the site of measurement in larger arteries is much farther from the wall than the very short (<5 μm) length of the glycocalyx (Reitsma et al., 2007).

Much of the twentieth century literature includes the idea that WSS has a narrow 'set-point' range, typically ~10–20 dyne cm^{-2}, throughout the circulatory system (Glagov et al., 1988; Ku, 1997). However, Langille realized that WSS in any particular artery is dependent on body mass (M_b; kg) (Langille, 1993). Based on his assumed scaling of cardiac output ($\propto M_b^{0.8}$) and geometrically proportional scaling of arterial linear dimension ($\propto$

$M_b^{0.33}$), he calculated that aortic WSS should scale allometrically with $M_b^{-0.2}$. More recently, data from mouse to human indicated that WSS scales with $M_b^{-0.38}$ for the infrarenal aorta (Greve et al., 2006; Weinberg and Ethier, 2007), $M_b^{-0.23}$ for the common carotid artery (from Fig. 2 in (Cheng et al., 2007)), and $M_b^{-0.21}$ for the common carotid artery (from data in (Weinberg and Ethier, 2007)). For primates, WSS appears to scale with $M_b^{-0.20}$ for the internal carotid artery (Seymour et al., 2015) and $M_b^{-0.22}$ for the vertebral artery (Boyer and Harrington, 2018a).

Few studies consider the scaling of both the anatomy and the physiology of the cardiovascular system of mammals. In a now classic paper, Holt and colleagues measured the sizes of the main arteries and veins of seven species of mammals ranging in body mass from mice (~0.02 kg) to horses and cows (~500 kg) (Holt et al., 1981). The internal radius (r_i; cm) of the ascending aorta scaled with body mass according to $r_i = 0.33\ M_b^{0.36}$. The authors estimated the scaling of cardiac output to be proportional to $M_b^{0.79}$ and, since radius scaled with $M_b^{0.36}$, radius squared (proportional to aortic cross sectional area) scaled with $M_b^{0.72}$, and therefore the mean velocity of the blood scaled with $M_b^{(0.79-0.72)} = M_b^{0.07}$. Although the authors concluded that mean blood velocity is body-mass-independent, the exponent of 0.07 produces a doubling of velocity between the mice and the horses and cows. WSS is also shown to decrease in the same artery of larger species; assuming that $\tau \propto \dot{Q}/r^3$, then $\tau \propto M_b^{(0.79-(3\times0.36)} = M_b^{-0.29}$.

In the present study, we hypothesized that the negative scaling of WSS with body mass is due to differences in the scaling of metabolic rate that would be reflected in the blood flow rates and the morphology of the arterial system. Rather than approaching the question from a theoretical model of fractal branching, we used an empirical approach to gather data from recent imaging studies of blood flow rate and arterial lumen size. This meta-study was designed to determine if there are patterns of blood flow rate and WSS in relation to *in vivo* arterial size among mammals over a wide range of body mass, and to determine if blood flow rate is associated with whole-body basal metabolic rate, independent of body mass. The unexpected finding of our meta-study is that allometric equations can be used to estimate blood flow rates in mammalian arteries from their radius alone, without reference to theoretical equations, or knowledge of wall shear stress, metabolic rate or body mass.

METHODS

Data collection

Recent advancements in ultrasonic, X-ray and magnetic resonance imaging, allowed us to collect data on systemic arterial radii and blood flow rates in mammals. The literature was searched for individual studies that included both pressurized internal radius and volume blood flow rate in the same arteries and the same species. All studies that presented data for both variables together were accepted, and none were excluded. No record was made of the number of searched papers that failed to present data for both variables. However, because the literature was strongly biased toward human studies, followed by laboratory rodents, a deliberate effort was made to search for other species.

Arterial lumen size and volume blood flow rate were taken as reported means from control groups. In some instances, flow rate was calculated from mean velocity multiplied by cross sectional lumen area. Arterial radius was calculated from either reported diameter or cross-sectional area, assuming the geometry of a perfect circle. WSS was calculated from the Poiseuille shear stress equation, given in the Introduction, assuming a constant blood viscosity of 0.04 dyne s cm^{-2} (Amin and Sirs, 1985; Schmid-Schönbein et al., 1969). There was good correlation between WSS calculated this way and values reported in some individual studies that used the derivative of near-wall blood velocity gradients. Flow in a given artery was considered constant, laminar and Newtonian. Turbulent flow occurs only occasionally for the descending aorta or near a stenosis, valve or aneurysm (Winkel et al., 2015), so such conditions were excluded. Most animal studies involved some level of general anesthesia or sedation, in which case the anesthetic was recorded. Data from exercising animals were also recorded but excluded from the dataset because too few records were available. Body masses were taken from individual studies, either as a reported mean, or as the average of a reported range. Missing body mass data were replaced with means from laboratory and domestic species (Jones et al., 2009; Seymour and Blaylock, 2000). Data for basal metabolic rate (BMR) were taken from a published compilation (Sieg et al., 2009) and supplemented with additional data for horses (Eisenberg, 1981; Evans and Rose, 1988). BMR data for crab-eating macaques *Macaca fascicularis* were unavailable, so BMR data for similarly-sized rhesus macaques *M. mulatta* were substituted.

Statistics

Values are presented as means with 95% confidence intervals (CI), calculated with Microsoft Excel add-in StatistiXL (www.statistixl.com). Data for $\dot{Q}$, r_i, τ, M_b and BMR were $\log_{10}$-transformed for analysis. Polynomial or power regression equations were fitted with graphing and statistical software (GraphPad Software Inc., La Jolla, CA, USA). The relationships between $\dot{Q}$, M_b and BMR were analysed using linear mixed models with species identity as a random effect in the lme4 v1.1-7 (Bates et al., 2014) and lmerTest v2.0-25 (Kuznetsova et al., 2015) packages of R v3.1.3 (R Core Team, 2015). The significance of fixed effects was assessed using t-tests with Satterthwaite approximations to degrees of freedom and models fitted using maximum likelihood. One value for rats was excluded from this analysis, because the individuals for which blood flow rate was determined were much smaller (100 g) than the individuals for which BMR was determined (290 g). For the remaining species, the log body masses of animals used for blood flow rate measurement were strongly correlated with the log body masses of animals used for metabolic rate measurement ($R^2 = 0.99$).

RESULTS

Blood flow rate and WSS in relation to arterial size

Data for arterial blood flow rate and lumen radius were obtained from 50 studies that included both variables in the same paper and were measured from mammals at rest (see Electronic supplementary material). The nine species comprised *Homo sapiens* and various domesticated or laboratory mammals. In total, there were 92 data points collected from 20 named systemic arteries. Body mass ranged from 23 g mice to 652 kg cows. Lumen radius varied between 3.65 µm in a cremaster artery of a rat to 11.2 mm in the supraceliac aorta of a human. Blood flow rate ranged from 0.16 μm^3 s^{-1} in the cremaster artery in a rat to 20 cm^3 s^{-1} in the femoral artery of a horse.

The entire dataset is described by a single second-order polynomial equation relating log blood flow rate to log lumen radius: $\log \dot{Q} = -0.20 \log r_i^2 + 1.91 \log r_i + 1.82$ ($R^2 = 0.97$; n = 92) (Fig. 1). The derivative (slope of the line at any point) of this equation reveals a gradual increase in slope with decreasing arterial size, from approximately 2 in the largest arteries to approximately 3 in the smallest ones.

WSS is normally calculated according to the assumption of laminar flow with the Poiseuille shear stress equation, given in the Introduction. The data show increasing WSS from 1.1 dyne cm^{-2} in the infrarenal aorta of humans to 163 dyne cm^{-2} in the small

cremaster artery of a rat (Fig. 2). A polynomial equation set to the data is $\log \tau = -0.20 \log r_i^2 -1.09 \log r_i + 0.53$ ($R^2 = 0.62$; n = 92).

Blood flow rate in the cephalic arteries only

A subset of the data was selected to include only the major cephalic arteries, because the blood flow regimes in these vessels are relatively constant (Fig. 3). These include the common carotid, internal carotid, vertebral, basilar, anterior cerebral, middle cerebral and posterior cerebral arteries. An allometric power regression was set to these data yielding the equation, $\dot{Q} = 155\ r_i^{2.49 \pm 0.17}$ ($R^2 = 0.94$; n = 57). The exponent is midway between 2 and 3 of the entire dataset.

Effect of body mass on blood flow rate and wall shear stress in the femoral artery, aorta and common carotid artery

Three major arteries provided sufficient data to relate resting $\dot{Q}$ to M_b allometrically (Fig. 4). The exponents are 0.80 for the femoral artery, 0.74 for the aorta and 0.80 for the common carotid artery. WSS calculated for these arteries yield exponents of -0.49 for the femoral artery, -0.44 for the aorta and -0.14 for the common carotid artery (Fig. 5). See captions to Figs 4 and 5 for complete equations.

Effect of basal metabolic rate (BMR) on blood flow rate in the common carotid artery

For species in which data on common carotid artery $\dot{Q}$ were available, we found that their whole-body BMR (ml O_2 h^{-1}) scales as $6.09\ M_b^{0.71 \pm 0.07}$. Common carotid artery $\dot{Q}$ ($cm^3\ s^{-1}$) scales as $0.24\ M_b^{0.80 \pm 0.09}$ and as $0.000157\ BMR^{1.11 \pm 0.09}$. The correlation between common carotid artery $\dot{Q}$ and BMR remains positive and significant ($t_{11.6} = 3.49$, p = 0.005) (Fig. 6), after accounting for the effect of M_b on $\dot{Q}$, which is not significant in the model that includes BMR ($t_{11.6} = -0.90$, p = 0.38), $\log \dot{Q} = -4.90 + 1.49 \log BMR - 0.279 \log M_b$. The effect of whole-body BMR on common carotid artery $\dot{Q}$ remains significant ($t_{30} = 3.60$, p = 0.001) in a model that includes vessel radius (r_i, $t_{30} = 2.14$, p = 0.04) and M_b ($t_{30} = -1.53$, p = 0.14), $\log \dot{Q} = -3.02 + 1.23 \log BMR + 1.03 \log r_i - 0.411 \log M_b$.

DISCUSSION

Blood flow rate and arterial size in resting mammals

The data gathered from 20 different systemic arteries in nine species of mammals differing in body mass by 4.5 orders of magnitude fall remarkably along a single, second-order polynomial regression line (Fig. 1). This close relationship is not simply a result of the influence of body mass. Although body mass is related to the size of individual named arteries, the six smallest arteries in the data set include rats, cats and humans that differ greatly in body mass. The relationship between $\dot{Q}$ and r_i is curved, with the derivative decreasing from a slope of approximately 2 in the largest arteries to about 3 in the smallest ones. The pattern is also apparent in different-sized arteries from humans and rats (Fig. 1). The explanation for this phenomenon has been sought in the following theoretical models.

The circulatory system has been analysed as a fractal-like branching network. Although the distal arteries appear to be close to geometrically dichotomously self-similar at every level (Family et al., 1989), the proximal arteries are not fractal, branching is not uniform, and arterial anastomoses occur (Huo and Kassab, 2016). There are two classical models for anatomical branching pattern of the arterial tree. The first is the minimum energy loss hypothesis known as Murray's Law, which predicts that $\dot{Q} \propto r^3$, such that r^3 of a parent artery is equal to the sum of r^3 of two daughter arteries (Murray, 1926). The other model, known as da Vinci's Rule because the anatomist and artist Leonardo da Vinci recorded that the cross-sectional area of a parent artery is equal to the combined areas of the daughter arteries (Richter, 1970), predicts that $\dot{Q} \propto r^2$ (Zamir et al., 1992). Both are cases of the common relationship, $r_p{}^n = r_{d1}{}^n + r_{d2}{}^n$, where r_p is the radius of the parent artery and r_{d1} and r_{d2} are the radii of the two daughter arteries. The exponent, n, is 3 for Murray's Law and 2 for da Vinci's Rule.

The present study shows that neither model holds for the entire arterial system. Rather, Murray's Law applies to the smaller arteries, as the derivative of the regression is close to 3, but da Vinci's Rule applies to the larger arteries, where the derivative is approximately 2. These results confirm other indications from the literature. For example, in small arteries, $\dot{Q} \propto r^{2.76}$ in human retinal arteries (Riva et al., 1985), similar to retinal arteries of rhesus monkeys (Zamir and Medeiros, 1982), $\dot{Q} \propto r^{3.01}$ in the cremaster muscle arteries of rats (Mayrovitz and Roy, 1983), and $\dot{Q} \propto r^{2.98}$ in pial arteries on the surface of the brain of cats (Kobari et al., 1984).

For the larger arteries, several studies conclude that $\dot{Q}$ should be proportional to radius squared. A meta-study of five species of mammals indicated that WSS is related to arterial diameter to the -0.50 power, which indicates that $\dot{Q} \propto r^{2.5}$ (Cheng et al., 2007).

Zamir et al. (1992) measured diameters in casts made from human central arteries and found that n is closer to 2 than 3. An intraspecific analysis of all major arteries with 3 – 10 branch levels in the human head and torso revealed high variability, but a mean empirical exponent equivalent to 2.04 or 2.44, depending on the estimation model employed (Newberry et al., 2015). The exponents for arterial size of vascular trees in organs of humans and laboratory animals range widely, approximately from 2 to 4 (Kassab, 2006). An alternative model to Murray's Law, but also based on fractal-like branching of the arterial tree with minimal energy loss, concludes that the exponent is between 2 and 3 (Huo and Kassab, 2016).

The shift from da Vinci's Rule in larger arteries to Murray's Law in the small ones has been explained in theoretical studies (Savage et al., 2008; West et al., 1997; West et al., 1999). The area-preserving relationship of da Vinci's Rule (where exponent n = 2) ensures that energy loss by reflected pressure waves is minimized in the major arteries (Gafiychuk and Lubashevsky, 2001). If the mean velocity in the parent is equal to the mean velocity in the daughters, and the wall characteristics are the same in the parent and daughters, then changes in velocity at the junction are not converted to reflected waves (Caro et al., 2012). Murray's Law (where exponent n = 3) minimizes frictional-related energy loss, because wall shear stress is equal in parent and daughter arteries, and permits the velocity of the blood to slow down at the level of the capillaries to allow sufficient time for gas exchange.

Scaling of blood flow rate and arterial size in the cephalic arteries only

The entire data set contains arteries that service tissues of varying metabolic rate. In particular, the inferior aorta, femoral arteries and brachial arteries largely supply skeletal muscles, while the common carotid and vertebral arteries and their branches supply mainly the brain. Flow regimes in these two categories are vastly different. For instance, flow rate in the femoral artery can increase 10-fold between rest and activity (Jorfeldt and Wahren, 1971). Therefore, the diameter of the femoral artery is matched better with maximum flow rate than resting flow rate. In contrast to muscle perfusion, brain perfusion is autoregulated and relatively constant globally, although there may be regional redistribution of blood (Ogoh and Ainslie, 2009; Payne, 2016). For example, blood flow rate in the common carotid artery of humans is independent of heart rate (Wilcox et al., 1970). During moderate, steady-state cycling exercise that causes a doubling of cardiac output, global cerebral blood flow rate increases only 28% above resting rates after 3 min and returns to resting rates after 13 min of continuing exercise (Hiura et al., 2014). Blood flow rate in the middle cerebral and internal carotid arteries increases by only 14% and 17%, respectively, despite doubling of heart rate during moderate cycling exercise (at 60-67% of maximal aerobic capacity), and the increase in blood flow rate along these arteries is even less during more

intense cycling exercise (80-90% of maximal aerobic capacity) (Hellström et al., 1996). In a similar experiment, Japanese women increased cardiac output by 260% during moderate cycling exercise, but increased internal carotid arterial flow rate by only 18% and vertebral artery flow by 33% (Sato and Sadamoto, 2010). The diameters of the cerebral arteries also change very little between rest and activity (Hellström et al., 1996) or in response to changes in blood pressure and blood gas levels (Payne, 2016). There is also almost no difference in cerebral blood flow rate when humans engage in mental arithmetic (Sokoloff et al., 1955) or between awake and sleeping states (Townsend et al., 1973). Cerebral blood flow rate of humans decreases gradually with age in absolute terms, but not when expressed relative to brain mass, despite rising arterial blood pressure (Meltzer et al., 2000; Tarumi and Zhang, 2018; van Es et al., 2010). However, cerebral blood flow rate in humans is responsive to short-term experimental alterations in mean arterial blood pressure (Tan, 2012; Willie et al., 2014), defending more strongly against increases in pressure than decreases (Numan et al., 2014).

The relationship between blood flow rate and arterial size in the cephalic arteries is best described by an allometric power equation (Fig. 3). The relationship is determined mainly by the data for the common carotid arteries from a 27 g mouse to a 500 kg horse. The exponent of the equation is 2.49 and the 95% CI of the exponent is 0.17. Thus, the exponent lies midway between, but is significantly different from, those expected for da Vinci's Rule (where n = 2) and Murray's Law (where n = 3).

Wall shear stress in relation to arterial size and body mass

The general trend in this meta-study indicates that WSS increases as blood passes into progressively smaller arteries (Fig. 2), in contrast to a generally assumed independence of WSS from vessel size and body mass according to Murray's Law. Thus our results from 50 studies of nine species of mammals confirms the pattern from seven studies of five species of mammals, which showed that WSS in the common carotid artery increases from approximately 11 to 65 dyne cm^{-2} from humans to mice (Cheng et al. 2007). Our data indicate an increase from 14 to 42 dyne cm^{-2} over the same body mass range.

Blood flow rate in three major arteries scales with body mass with exponents between 0.74 and 0.80 (Fig. 4), which is consistent with the scaling of cardiac output in resting mammals, ca. 0.80 (Calder, 1996; Holt et al., 1981). Calculated WSS in these arteries decreases with increasing body mass, with large negative exponents in the femoral artery (-0.49) and aorta (-0.44), but a smaller negative exponent in the common carotid artery (-0.14) (Fig. 5). By comparison, the exponent was reported to be -0.38 in the aorta (Greve et al., 2006; Weinberg and Ethier, 2007) and between -0.20 and -0.23 in the common carotid, internal carotid and vertebral arteries (Boyer and Harrington, 2018a; Cheng et al., 2007;

Greve et al., 2006; Seymour et al., 2015; Weinberg and Ethier, 2007). This may represent a decreased sensitivity of WSS to body size in arteries that supply mainly nervous tissue as opposed to arteries that supply a large fraction of blood to muscles during activity, but are measured at rest. In fact, WSS is quite low in the femoral artery at rest, but increases during activity to be comparable to those in the similarly-sized common carotid artery at rest (Kornet et al., 2000).

The standard shear stress equation assumes that WSS is inversely proportional to r_i^3. If $\dot{Q}$ is also proportional to r_i^3, then WSS is a constant (i.e., $\tau \propto r_i^0$). If $\dot{Q}$ is proportional to r_i^2, then WSS should increase in smaller arteries ($\tau \propto r_i^{-1}$), which appears to be the case (Fig. 2). However, we found that the exponent in fact varies between 3 and 2 depending on arterial size, so we can calculate wall shear stress according to a modified shear stress equation, $\tau = (4\,\dot{Q}\,\eta)/(\pi\,r_i^n)$, where n is the derivative of the polynomial equation for $\dot{Q}$ and r_i. The descriptive equation for the curve based on the derivative is $\log \tau = 0.200 \log r_i^2 - 0.017 \log r_i + 0.530$ ($R^2 = 0.70$; n = 92) (Electronic supplementary material Fig. S1). This modified equation also shows that WSS increases with decreasing arterial size, from nearly 3 dyne cm^{-2} in the largest arteries to above 1500 dyne cm^{-2} in the cremaster arteries of rats, which is certainly unrealistically high. All of the calculations of WSS should be approached with caution for three reasons. First, the standard equation assumes that WSS is inversely proportional to r_i^3, which is doubtful. Second, they are based on flow rates during rest, but flow rates in large arteries supplying muscles can increase greatly, without a complete compensatory increase in radius (Cheng et al., 2003). Third, they assume that blood viscosity is constant, but the effective viscosity near the wall of the smallest arteries might be reduced (Sriram et al., 2014).

Blood flow rate in relation to basal metabolic rate

The most represented artery in the dataset is the common carotid artery. When the effect of body mass is accounted for, there is a positive relationship between common carotid artery blood flow rate and whole-body BMR (Fig. 6). This implies that species with higher BMR also have higher cephalic perfusion rates and brain metabolic rates. This positive relationship is similar to the relationship observed between brain size and metabolic rate in several studies of eutherian mammals. Body-mass-independent brain size is positively correlated with body-mass-independent metabolic rate in humans (Javed et al., 2010; Müller et al., 2011) and inbred strains of mice (Konarzewski and Diamond, 1995), and in eutherian mammals in general (Navarrete et al., 2011; Weisbecker and Goswami, 2010). In contrast, there is no relationship between brain size and metabolic rate in marsupials (Weisbecker and Goswami, 2010), birds (Isler and van Schaik, 2006), or teleost fishes (Killen et al., 2016).

The correlation between brain size and metabolic rate, where present, and the correlation between common carotid artery blood flow rate and whole body BMR, may arise because the brain is energetically expensive to maintain and contributes significantly to whole-body metabolism. The human brain is certainly expensive, accounting for around 20% of BMR, but the contribution is much smaller (2 - 8%) in most non-primate species (Mink et al., 1981), although there are some notable exceptions (Nilsson, 1996). The proximate cause of the relationship between body-mass-independent BMR and body-mass-independent brain size has long been controversial (McNab and Eisenberg, 1989). It may arise indirectly via extrinsic factors that influence both brain size and metabolic rate, rather than directly as a functional consequence of the contribution of the brain to whole-body metabolism (Glazier, 2018; McNab and Köhler, 2017; White and Kearney, 2013). It is possible that mammals with high BMR are generally more active and require greater ability to process sensory information quickly.

Practical use of the equations

If the size of the lumen of an artery subject to normal physiological blood pressures is known, the flow rate can be estimated. The second-order polynomial equation for the entire dataset (Fig. 1) is useful over the broad range of vessel size and can be applied loosely to any mammal, even if the destination of the arterial blood (e.g., neural or muscular) is not known. Because the flow rate in the cephalic arteries is rather constant, the power equation (Fig. 3) can be used more precisely to estimate blood flow rate to the brain. The usefulness of the equations is enhanced over previous attempts, because they do not involve adherence to theory ($\dot{Q} \propto r_i^3$), and there are no assumptions about the scaling of WSS on body mass. In particular, we previously used the relationship, $\dot{Q} = (\tau\,\pi\,r_i^3)/(4\,\eta)$, and assumed that $\tau = 167\,M_b^{-0.20}$, based on data from only humans and rats, to estimate blood flow rates through the internal carotid artery from the radius of the carotid foramen (Seymour et al., 2015). This assumption was tenuous, not only because it was based on just two species, but also because the functional relationship between WSS and body mass was quite obscure. This aspect of our method was criticized (Boyer and Harrington, 2018a), defended (Seymour and Snelling, 2018) and then supported (Boyer and Harrington, 2018b). With the present analysis, however, we can circumvent the issue altogether and not involve WSS or body mass. The new empirical equations apply well to a broad range of arteries over a broad range of body size under resting conditions, so they offer the prospect of estimating blood flow rate (and hence, oxygen delivery and metabolic rate) in organs according to the size of their supply arteries.

Author contributions

Conceptualization: R.S.S.; Data gathering: R.S.S.; Formal analysis: R.S.S., Q.H., C.R.W., E.P.S.; Writing - original draft: R.S.S.; Writing - review and editing: R.S.S., Q.H., C.R.W., E.P.S.; Project administration: R.S.S.

Supplementary information

Supplementary information available online at
http://jeb.biologists.org/lookup/doi/xxxxxxxx

References

   Amin, T. M. and Sirs, J. A. (1985). The blood rheology of man and various animal species. *Quarterly Journal of Experimental Physiology and Cognate Medical Sciences* **70**, 37-49.

   Baeyens, N., Nicoli, S., Coon, B. G., Ross, T. D., Van den Dries, K., Han, J., Lauridsen, H. M., Mejean, C. O., Eichmann, A., Thomas, J. L. et al. (2015). Vascular remodeling is governed by a VEGFR3-dependent fluid shear stress set point. *Elife* **4**, e04645

   Bates, D., Mächler, M., Bolker, B. and Walker, S. (2014). lme4: Linear mixed-effects models using Eigen and S4. R package version 1.1-7, <URL: https://CRAN.R-project.org/package=lme4>.

   Boyer, D. M. and Harrington, A. R. (2018a). Scaling of bony canals for encephalic vessels in euarchontans: Implications for the role of the vertebral artery and brain metabolism. *Journal of Human Evolution* **114**, 85-101.

   Boyer, D. M. and Harrington, A. R. (2018b). New estimates of blood flow rates in the vertebral artery of euarchontans and their implications for encephalic blood flow scaling: A response to Seymour and Snelling (2018). *Journal of Human Evolution* **In press**.

Boyer, D. M. and Harrington, A. R. (2018b). Scaling of bony canals for encephalic vessels in euarchontans: Implications for the role of the vertebral artery and brain metabolism. *Journal of Human Evolution* **114**, 85-101.

Brummer, A. B., Savage, V. M. and Enquist, B. J. (2017). A general model for metabolic scaling in self-similar asymmetric networks. *PLoS Computational Biology* **13**, e1005394.

Calder, W. A., III. (1996). Size, Function, and Life History. Mineola, New York: Dover Publications.

Caro, C. G., Pedley, T. J., Schroter, R. C. and Seed, W. A. (2012). The Mechanics of the Circulation. Cambridge: Cambridge University Press.

Cheng, C., Helderman, F., Tempel, D., Segers, D., Hierck, B., Poelmann, R., van Tol, A., Duncker, D. J., Robbers-Visser, D., Ursem, N. T. C. et al. (2007). Large variations in absolute wall shear stress levels within one species and between species. *Atherosclerosis* **195**, 225-235.

Cheng, C. P., Herfkens, R. J. and Taylor, C. A. (2003). Abdominal aortic hemodynamic conditions in healthy subjects aged 50-70 at rest and during lower limb exercise: *in vivo* quantification using MRI. *Atherosclerosis* **168**, 323-331.

Eisenberg, J. F. (1981). The Mammalian Radiations: An Analysis of Trends in Evolution, Adaptation, and Behavior. Chicago: University of Chicago Press.

Evans, D. L. and Rose, R. J. (1988). Dynamics of cardiorespiratory function in standardbred horses during different intensities of constant-load exercise. *Journal of Comparative Physiology B* **157**, 791-799.

Family, F., Masters, B. R. and Platt, D. E. (1989). Fractal pattern formation in human retinal vessels. *Physica D* **38**, 98-103.

Gafiychuk, V. V. and Lubashevsky, I. A. (2001). On the principles of the vascular network branching. *Journal of Theoretical Biology* **212**, 1-9.

Glagov, S., Zarins, C., Giddens, D. P. and Ku, D. N. (1988). Hemodynamics and atherosclerosis - insights and perspectives gained from studies of human arteries. *Archives of Pathology and Laboratory Medicine* **112**, 1018-1031.

Glazier, D. S. (2018). Rediscovering and reviving old observations and explanations of metabolic scaling in living systems. *Systems* **6**, e 6010004.

Greve, J. M., Les, A. S., Tang, B. T., Blomme, M. T. D., Wilson, N. M., Dalman, R. L., Pelc, N. J. and Taylor, C. A. (2006). Allometric scaling of wall shear stress from mice to humans: quantification using cine phase-contrast MRI and computational fluid dynamics. *American Journal of Physiology. Heart and Circulatory Physiology* **291**, H1700-H1708.

Heil, M., Eitenmuller, I., Schmitz-Rixen, T. and Schaper, W. (2006). Arteriogenesis versus angiogenesis: similarities and differences. *Journal of Cellular and Molecular Medicine* **10**, 45-55.

Hellström, G., Fischer-Colbrie, W., Wahlgren, N. G. and Jogestrand, T. (1996). Carotid artery blood flow and middle cerebral artery blood flow velocity during physical exercise. *Journal of Applied Physiology* **81**, 413-418.

Hillman, S. S. and Hedrick, M. S. (2015). A meta-analysis of *in vivo* vertebrate cardiac performance: implications for cardiovascular support in the evolution of endothermy. *Journal of Experimental Biology* **218**, 1143-1150.

Hiura, M., Nariai, T., Ishii, K., Sakata, M., Oda, K., Toyohara, J. and Ishiwata, K. (2014). Changes in cerebral blood flow during steady-state cycling exercise: a study using

oxygen-15-labeled water with PET. *Journal of Cerebral Blood Flow and Metabolism* **34**, 389-396.

Holt, J. P., Rhode, E. A., Holt, W. W. and Kines, H. (1981). Geometric similarity of aorta, venae cavae, and certain of their branches in mammals. *American Journal of Physiology. Regulatory, Integrative and Comparative Physiology* **241**, 100-104.

Hunt, D. and Savage, V. M. (2016). Asymmetries arising from the space-filling nature of vascular networks. *Physical Review E* **93**.

Huo, Y. and Kassab, G. S. (2012). Intraspecific scaling laws of vascular trees. *Journal of The Royal Society Interface* **9**, 190-200.

Huo, Y. L. and Kassab, G. S. (2016). Scaling laws of coronary circulation in health and disease. *Journal of Biomechanics* **49**, 2531-2539.

Isler, K. and van Schaik, C. (2006). Costs of encephalization: the energy trade-off hypothesis tested on birds. *Journal of Human Evolution* **51**, 228-43.

Javed, F., He, Q., Davidson, L. E., Thornton, J. C., Albu, J., Boxt, L., Krasnow, N., Elia, M., Kang, P., Heshka, S. et al. (2010). Brain and high metabolic rate organ mass: contributions to resting energy expenditure beyond fat-free mass. *American Journal of Clinical Nutrition* **91**, 907-912.

Jones, K. E., Bielby, J., Cardillo, M., Fritz, S. A., O'Dell, J., Orme , C. D. L., Safi, K., Sechrest, W., Boakes, E. H., Carbone, C. et al. (2009). PanTHERIA: a species-level database of life history, ecology, and geography of extant and recently extinct mammals. *Ecology* **90**, 2648.

Jorfeldt, L. and Wahren, J. (1971). Leg blood flow during exercise in man. *Clinical Science* **41**, 459-473.

Kamiya, A., Bukhari, R. and Togawa, T. (1984). Adaptive regulation of wall shear stress optimizing vascular tree function. *Bulletin of Mathematical Biology* **46**, 127-137.

Kamiya, A. and Togawa, T. (1980). Adaptive regulation of wall shear stress to flow change in the canine carotid artery. *American Journal of Physiology. Heart and Circulatory Physiology* **239**, H14-H21.

Kassab, G. S. (2006). Scaling laws of vascular trees: of form and function. *American Journal of Physiology. Heart and Circulatory Physiology* **290**, H894-H903.

Killen, S. S., Glazier, D. S., Rezende, E. L., Clark, T. D., Atkinson, D., Willener, A. S. T. and Halsey, L. G. (2016). Ecological influences and morphological correlates of resting and maximal metabolic rates across teleost fish species. *American Naturalist* **187**, 592-606.

Kobari, M., Gotoh, F., Fukuuchi, Y., Tanaka, K., Suzuki, N. and Uematsu, D. (1984). Blood flow velocity in the pial arteries of cats, with particular reference to the vessel diameter. *Journal of Cerebral Blood Flow and Metabolism* **4**, 110-114.

Konarzewski, M. and Diamond, J. (1995). Evolution of basal metabolic rate and organ masses in laboratory mice. *Evolution* **49**, 1239-1248.

Kornet, L., Hoeks, A. P. G., Lambregts, J. and Reneman, R. S. (2000). Mean wall shear stress in the femoral arterial bifurcation is low and independent of age at rest. *Journal of Vascular Research* **37**, 112-122.

Kozłowski, J. and Weiner, J. (1997). Interspecific allometries are by-products of body size optimization. *American Naturalist* **149**, 352-380.

Ku, D. N. (1997). Blood flow in arteries. *Annual Review of Fluid Mechanics* **29**, 399-434.

Kuznetsova, A., Brockhoff, P. B. and Christensen, R. H. B. (2015). lmerTest: Tests in Linear Mixed Effects Models. R package version 2.0-25. http://CRAN.R-project.org/package=lmerTest.

Langille, B. L. (1993). Remodeling of developing and mature arteries: Endothelium, smooth-muscle, and matrix. *Journal of Cardiovascular Pharmacology* **21**, S11-S17.

Langille, B. L. (1999). Fluid dynamics in vascular pathology: adaptations of the arterial wall to chronic changes in blood flow. *Journal of Vascular Surgery* **29**, 1106-1108.

Lehoux, S., Castier, Y. and Tedgui, A. (2006). Molecular mechanisms of the vascular responses to haemodynamic forces. *Journal of Internal Medicine* **259**, 381-392.

Lehoux, S. and Tedgui, A. (2003). Cellular mechanics and gene expression in blood vessels. *Journal of Biomechanics* **36**, 631-643.

Lu, D. S. and Kassab, G. S. (2011). Role of shear stress and stretch in vascular mechanobiology. *Journal of The Royal Society Interface* **8**, 1379-1385.

Mayrovitz, H. N. and Roy, J. (1983). Microvascular blood-flow: Evidence indicating a cubic dependence on arteriolar diameter. *American Journal of Physiology. Heart and Circulatory Physiology* **245**, 1031-1038.

McNab, B. K. and Eisenberg, J. F. (1989). Brain size and its relation to the rate of metabolism in mammals. *American Naturalist* **133**, 157-167.

McNab, B. K. and Köhler, M. (2017). The difficulty with correlations: Energy expenditure and brain mass in bats. *Comparative Biochemistry and Physiology Part A: Molecular & Integrative Physiology* **212**, 9-14.

Meltzer, C. C., Cantwell, M. N., Greer, P. J., Ben-Eliezer, D., Smith, G., Frank, G., Kaye, W. H., Houck, P. R. and Price, J. C. (2000). Does cerebral blood flow decline in healthy aging? A PET study with partial-volume correction. *Journal of Nuclear Medicine* **41**, 1842-1848.

Mink, J. W., Blumenschine, R. J. and Adams, D. B. (1981). Ratio of central nervous system to body metabolism in vertebrates: its constancy and functional basis. *American Journal of Physiology-Regulatory, Integrative and Comparative Physiology* **241**, R203-R212.

Müller, M. J., Langemann, D., Gehrke, I., Later, W., Heller, M., Glüer, C. C., Heymsfield, S. B. and Bosy-Westphal, A. (2011). Effect of constitution on mass of individual organs and their association with metabolic rate in humans—a detailed view on allometric scaling. *Plos One* **6**, e22732.

Murray, C. D. (1926). The physiological principle of minimum work. I. The vascular system and the cost of blood volume. *Proceedings of the National Academy of Sciences of the United States of America* **12**, 207-214.

Navarrete, A., van Schaik, C. P. and Isler, K. (2011). Energetics and the evolution of human brain size. *Nature* **480**, 91-93.

Newberry, M. G., Ennis, D. B. and Savage, V. M. (2015). Testing foundations of biological scaling theory using automated measurements of vascular networks. *PLoS Computational Biology* **11**, e1004455.

Nilsson, G. E. (1996). Brain and body oxygen requirements of *Gnathonemus petersii*, a fish with an exceptionally large brain. *Journal of Experimental Biology* **199**, 603-607.

Numan, T., Bain, A. R., Hoiland, R. L., Smirl, J. D., Lewis, N. C. and Ainslie, P. N. (2014). Static autoregulation in humans: a review and reanalysis. *Medical Engineering and Physics* **36**, 1487-1495.

Ogoh, S. and Ainslie, P. N. (2009). Cerebral blood flow during exercise: mechanisms of regulation. *Journal of Applied Physiology* **107**, 1370-1380.

Owens, C. D. (2010). Adaptive changes in autogenous vein grafts for arterial reconstruction: Clinical implications. *Journal of Vascular Surgery* **51**, 736-746.

Papaioannou, T. G. and Stefanadis, C. (2005). Vascular wall shear stress: basic principles and methods. *Hellenic Journal of Cardiology* **46**, 9-15.

Payne, S. (2016). Cerebral Autoregulation: Control of Blood Flow in the Brain. Switzerland: Springer Nature.

Polet, F. and Feron, O. (2013). Endothelial cell metabolism and tumour angiogenesis: glucose and glutamine as essential fuels and lactate as the driving force. *Journal of Internal Medicine* **273**, 156-165.

Price, C. A., Enquist, B. J. and Savage, V. M. (2007). A general model for allometric covariation in botanical form and function. *Proceedings of the National Academy of Sciences of the United States of America* **104**, 13204-13209.

Prior, B. M., Yang, H. T. and Terjung, R. L. (2004). What makes vessels grow with exercise training? *Journal of Applied Physiology* **97**, 1119-1128.

R Core Team. (2015). R: A Language and Environment for Statistical Computing. Vienna, Austria: R Foundation for Statistical Computing.

Reitsma, S., Slaaf, D. W., Vink, H., van Zandvoort, M. and Egbrink, M. (2007). The endothelial glycocalyx: composition, functions, and visualization. *Pflugers Archiv-European Journal of Physiology* **454**, 345-359.

Richter, J. P. (1970). The Notebooks of Leonardo da Vinci. New York: Dover Publications.

Riva, C. E., Grunwald, J. E., Sinclair, S. H. and Petrig, B. L. (1985). Blood velocity and volumetric flow rate in human retinal vessels. *Investigative Ophthalmology and Visual Science* **26**, 1124-1132.

Sato, K. and Sadamoto, T. (2010). Different blood flow responses to dynamic exercise between internal carotid and vertebral arteries in women. *Journal of Applied Physiology* **109**, 864-869.

Savage, V. M., Deeds, E. J. and Fontana, W. (2008). Sizing up allometric scaling theory. *PLoS Computational Biology* **4**, e1000171.

Schmid-Schönbein, H., Wells, R. and Goldstone, J. (1969). Influence of deformability of human red cells upon blood viscosity. *Circulation Research* **25**, 131-143.

Seymour, R. S., Angove, S. E., Snelling, E. P. and Cassey, P. (2015). Scaling of cerebral blood perfusion in primates and marsupials. *Journal of Experimental Biology* **218**, 2631-2640.

Seymour, R. S. and Blaylock, A. J. (2000). The Principle of Laplace and scaling of ventricular wall stress and blood pressure in mammals and birds. *Physiological and Biochemical Zoology* **73**, 389-405.

Seymour, R. S. and Snelling, E. P. (2018). Calculating brain perfusion of primates. *Journal of Human Evolution* **in press**.

Sieg, A. E., O'Conner, M. P., McNair, J. N., Grant, B. W., Agosta, S. J. and Dunham, A. E. (2009). Mammalian metabolic allometry: do intraspecific variation, phylogeny, and regression models matter? *American Naturalist* **174**, 720-733.

Silvestre, J. S., Smadja, D. M. and Levy, B. I. (2013). Postischemic revascularization: From cellular and molecular mechanisms to clinical applications. *Physiological Reviews* **93**, 1743-1802.

Smiesko, V. and Johnson, P. C. (1993). The arterial lumen is controlled by flow-related shear stress. *News in Physiological Sciences* **8**, 34-38.

Sokoloff, L., Mangold, R., Wechsler, R. L., Kennedy, C. and Kety, S. S. (1955). Effect of mental arithmetic on cerebral circulation and metabolism. *Journal of Clinical Investigation* **34**, 1101-1108.

Sriram, K., Intaglietta, M. and Tartakovsky, D. M. (2014). Non-Newtonian flow of blood in arterioles: Consequences for wall shear stress measurements. *Microcirculation* **21**, 628-639.

Tan, C. O. (2012). Defining the characteristic relationship between arterial pressure and cerebral flow. *Journal of Applied Physiology* **113**, 1194-1200.

Tarumi, T. and Zhang, R. (2018). Cerebral blood flow in normal aging adults: cardiovascular determinants, clinical implications, and aerobic fitness. *Journal of Neurochemistry* **144**, 595-608.

Tekin, E., Hunt, D., Newberry, M. G. and Savage, V. M. (2016). Do vascular networks branch optimally or randomly across spatial scales? *PLoS Computational Biology* **12**, e1005223.

Thijssen, D. H. J., Cable, N. T. and Green, D. J. (2012). Impact of exercise training on arterial wall thickness in humans. *Clinical Science* **122**, 311-322.

Townsend, R. E., Prinz, P. N. and Obrist, W. D. (1973). Human cerebral blood flow during sleep and waking. *Journal of Applied Physiology* **35**, 620-625.

Tronc, F., Wassef, M., Esposito, B., Henrion, D., Glagov, S. and Tedgui, A. (1996). Role of NO in flow-induced remodeling of the rabbit common carotid artery. *Arteriosclerosis Thrombosis and Vascular Biology* **16**, 1256-1262.

van Es, A. C. G. M., van der Grond, J., ten Dam, V. H., de Craen, A. J. M., Blauw, G. J., Westendorp, R. G. J., Admiraal-Behloul, F. and van Buchem, M. A. (2010). Associations between total cerebral blood flow and age related changes of the brain. *Plos One* **5**, e9825.

Weinberg, P. D. and Ethier, C. R. (2007). Twenty-fold difference in hemodynamic wall shear stress between murine and human aortas. *Journal of Biomechanics* **40**, 1594-1598.

Weisbecker, V. and Goswami, A. (2010). Brain size, life history, and metabolism at the marsupial/placental dichotomy. *Proceedings of the National Academy of Sciences of the United States of America* **107**, 16216-16221.

West, G. B., Brown, J. H. and Enquist, B. J. (1997). A general model for the origin of allometric scaling laws in biology. *Science* **276**, 122-126.

West, G. B., Brown, J. H. and Enquist, B. J. (1999). The fourth dimension of life: fractal geometry and allometric scaling of organisms. *Science* **284**, 1677-1679.

White, C. R. and Kearney, M. R. (2013). Determinants of inter-specific variation in basal metabolic rate. *Journal of Comparative Physiology B* **183**, 1-26.

Wilcox, B., Coulter, N., Rackley, C. and Croom, R. (1970). The effect of changing heart rate on blood flow, power dissipation, and resistance in the common carotid artery of man. *Annals of Surgery* **171**, 24-30.

Willie, C. K., Tzeng, Y. C., Fisher, J. A. and Ainslie, P. N. (2014). Integrative regulation of human brain blood flow. *Journal of Physiology (London)* **592**, 841-859.

Winkel, L. C., Hoogendoorn, A., Xing, R. Y., Wentzel, J. J. and Van der Heiden, K. (2015). Animal models of surgically manipulated flow velocities to study shear stress-induced atherosclerosis. *Atherosclerosis* **241**, 100-110.

Wolinsky, H. and Glagov, S. (1967). A lamellar unit of aortic medial structure and function in mammals. *Circulation Research* **20**, 99-111.

Zamir, M. and Medeiros, J. A. (1982). Arterial branching in man and monkey. *Journal of General Physiology* **79**, 353-360.

Zamir, M., Sinclair, P. and Wonnacott, T. H. (1992). Relation between diameter and flow in major branches of the arch of the aorta. *Journal of Biomechanics* **25**, 1303-1310.
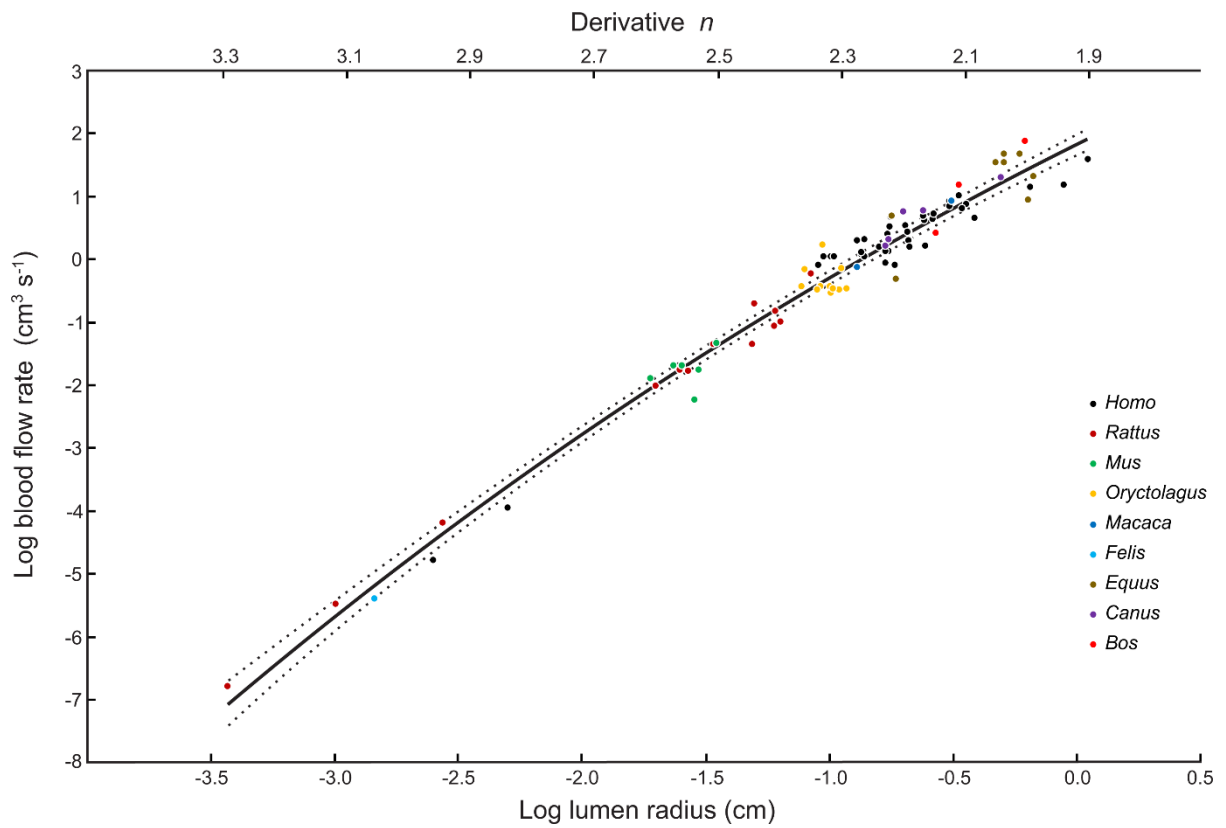
Figures

Figure 1. Relationship between log blood flow rate ($\dot{Q}$; cm^3 s^{-1}) and log systemic arterial lumen radius (r_i; cm) in nine genera of mammals at rest. The equation for the polynomial regression line is: log $\dot{Q}$ = -0.20 log r_i^2 +1.91 log r_i +1.82. 95% confidence bands for the regression line are shown. The value of the slope of the line at any point (derivative n) is given on the top axis.
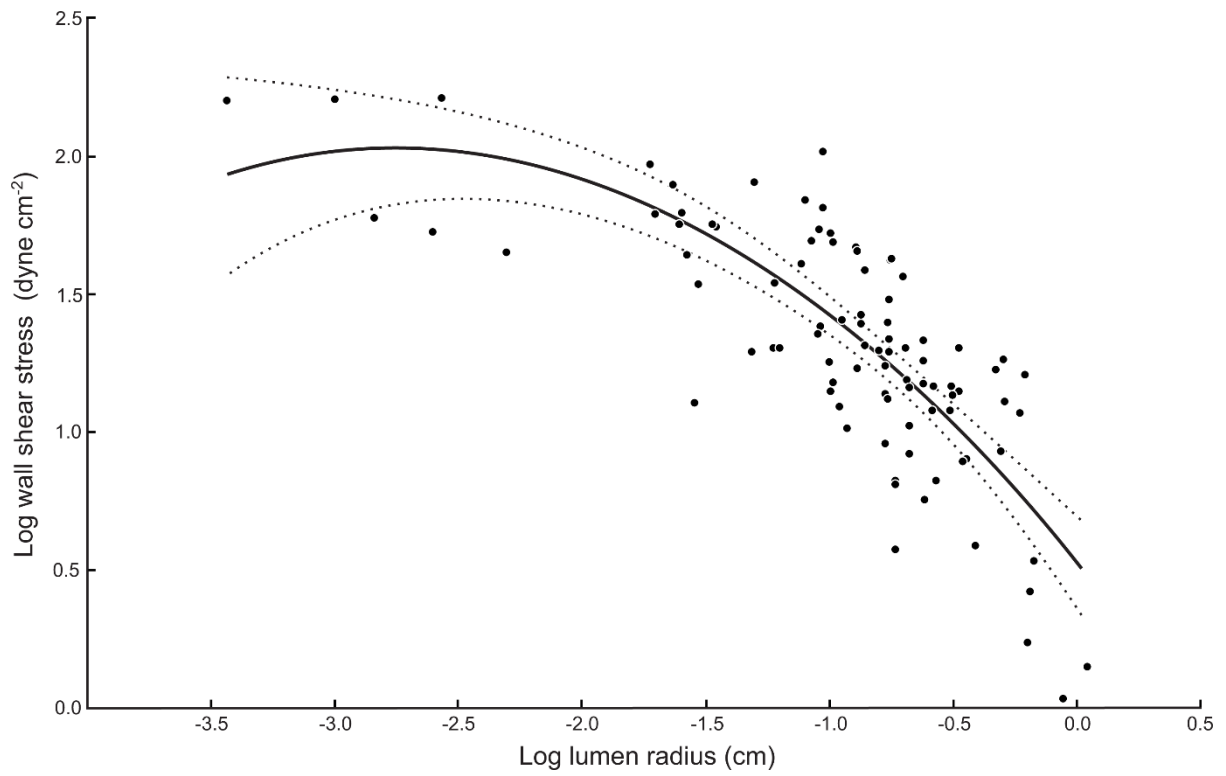
Figure 2. Relationship between log wall shear stress (τ; dyne cm^{-2}) and log systemic arterial lumen radius (r_i; cm) in mammals at rest, calculated from the Poiseuille shear stress equation, $\tau = (4\,\dot{Q}\,\eta)/(\pi\,r_i^3)$. The equation for the polynomial mean regression line is: $\log\tau = -0.20\,\log r_i^2 - 1.09\,\log r_i + 0.53$. 95% confidence bands for the regression line are shown.
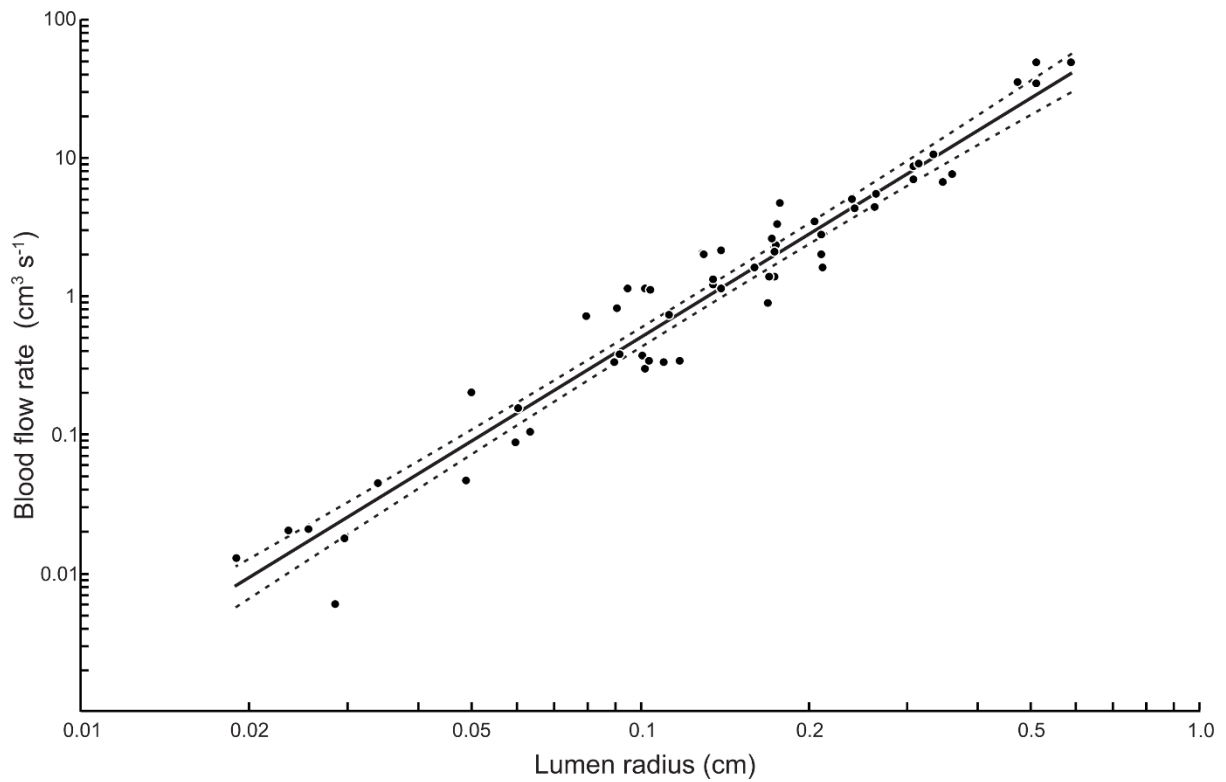
Figure 3. Subset of the data for blood flow rate ($\dot{Q}$; cm^3 s^{-1}) in relation to lumen radius (r_i; cm) in the major cephalic arteries only, including the common carotid, internal carotid, vertebral, basilar, anterior cerebral, middle cerebral and posterior cerebral arteries for six species of mammals (*Mus*, *Rattus*, *Oryctolagus*, *Canus*, *Homo*, *Equus*) at rest. The allometric equation for the power mean regression line of these arteries is $\dot{Q}$ = 155 $r_i^{2.49 \pm 0.17}$. 95% confidence bands for the regression line are shown. Note that arithmetic data are plotted on logged axes.
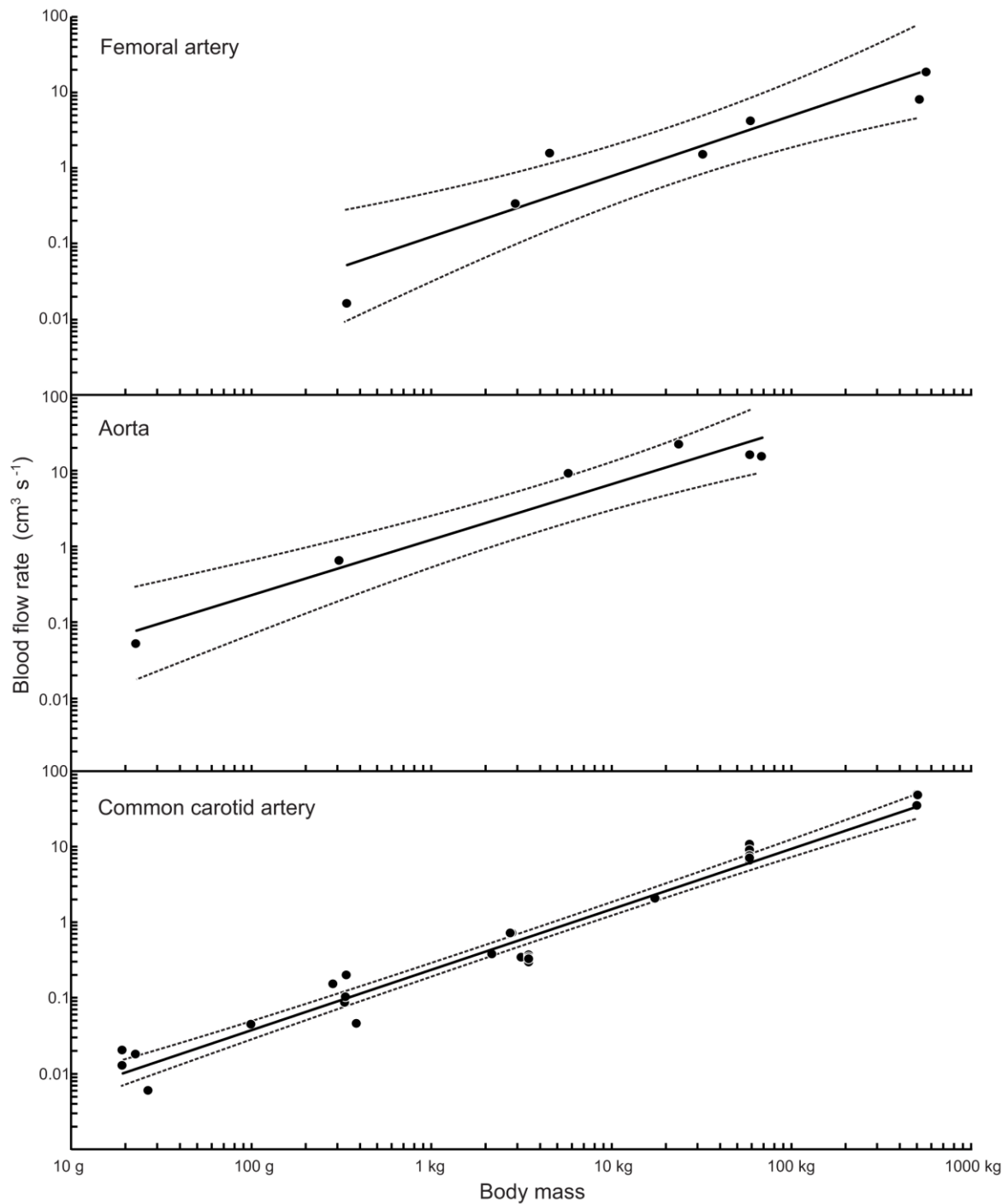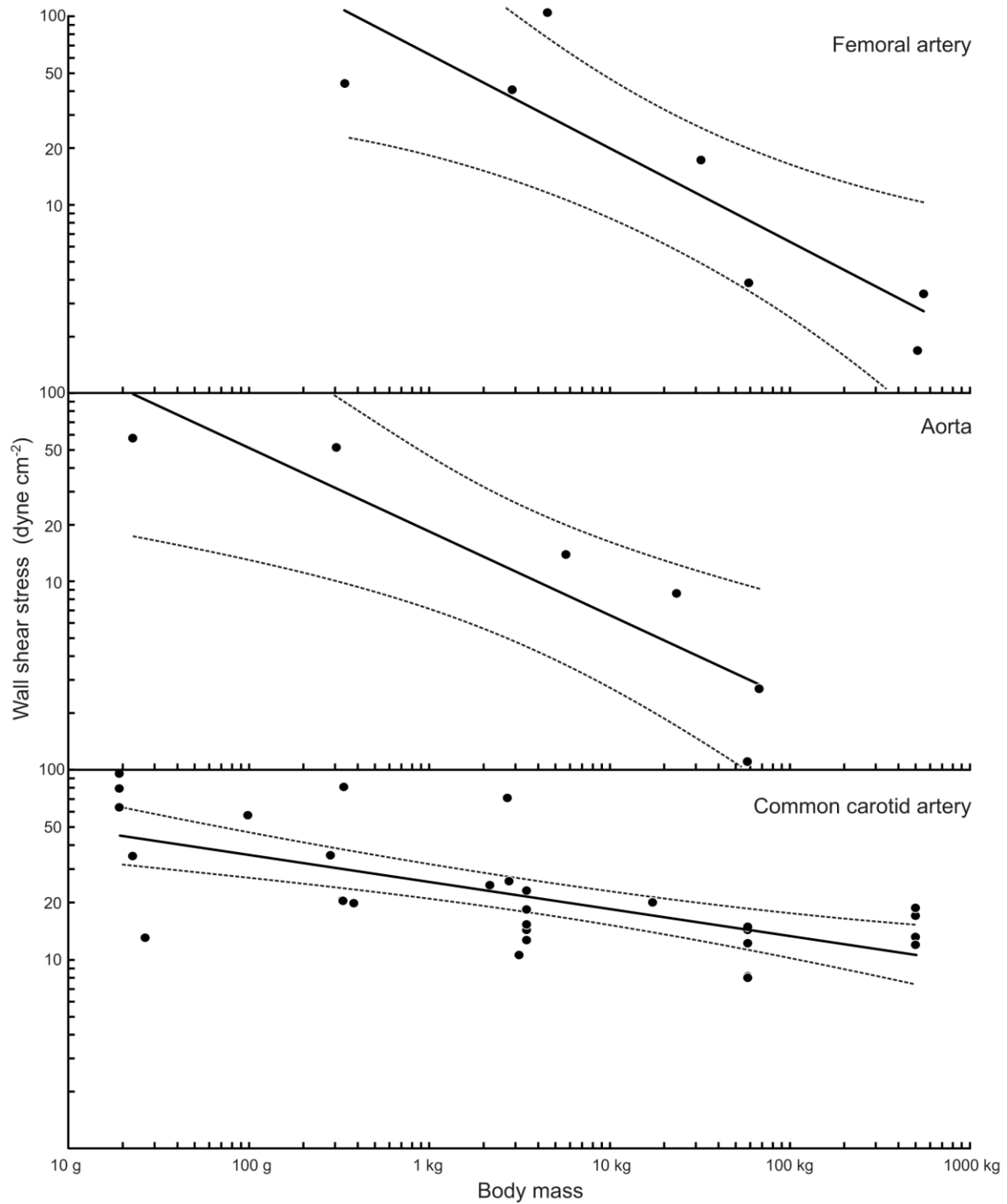
Figure 4.   Effect of body mass (M_b; kg) on blood flow rate ($\dot{Q}$; cm^3 s^{-1}) in three major arteries of mammals at rest. The allometric equations are: femoral artery, $\dot{Q}$ = 0.12 $M_b^{0.80\pm0.34}$ (R^2 = 0.88; n = 7); aorta, $\dot{Q}$ = 1.15 $M_b^{0.74\pm0.24}$ (R^2 = 0.95; n = 6); common carotid artery, $\dot{Q}$ = 0.24 $M_b^{0.80\pm0.06}$ (R^2 = 0.97; n = 31). 95% confidence bands for each regression line are shown. Note that arithmetic data are plotted on logged axes.
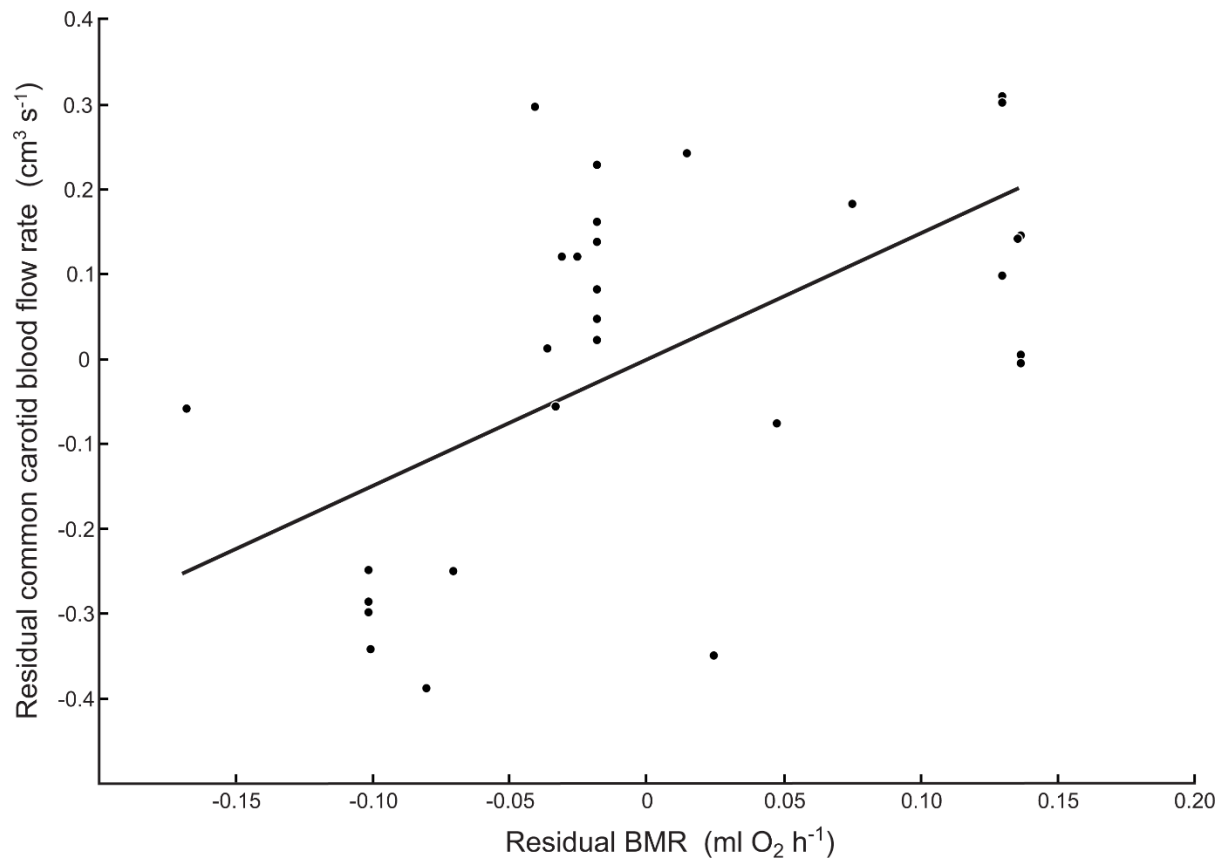
Figure 5. Effect of body mass (M_b; kg) on wall shear stress (τ; dyne cm^{-2}) in three major arteries of mammals at rest. The allometric equations are: femoral artery, $\tau = 61\ M_b^{-0.49\pm0.32}$ ($R^2 = 0.76$; n = 6); aorta, $\tau = 18\ M_b^{-0.44\pm0.29}$ ($R^2 = 0.82$; n = 7); common carotid artery, $\tau = 25\ M_b^{-0.14\pm0.06}$ ($R^2 = 0.45$; n = 31). 95% confidence bands for each regression line are shown. Note that arithmetic data are plotted on logged axes.

Figure 6. Relationship between the residuals of log common carotid artery blood flow rate ($\dot{Q}$, cm^3 s^{-1}) and the residuals of log whole-body basal metabolic rate (BMR, ml O_2 h^{-1}). Because both variables are significantly related to body mass (M_b, kg), residuals of each variable from linear regressions that relate $\dot{Q}$ and BMR to M_b are shown. The line represents the parameter estimate for the effect of BMR on $\dot{Q}$, accounting for M_b, in a linear mixed model including a random effect of species identity (log $\dot{Q}$ = -4.90 + 1.49 log BMR - 0.279 log M_b).
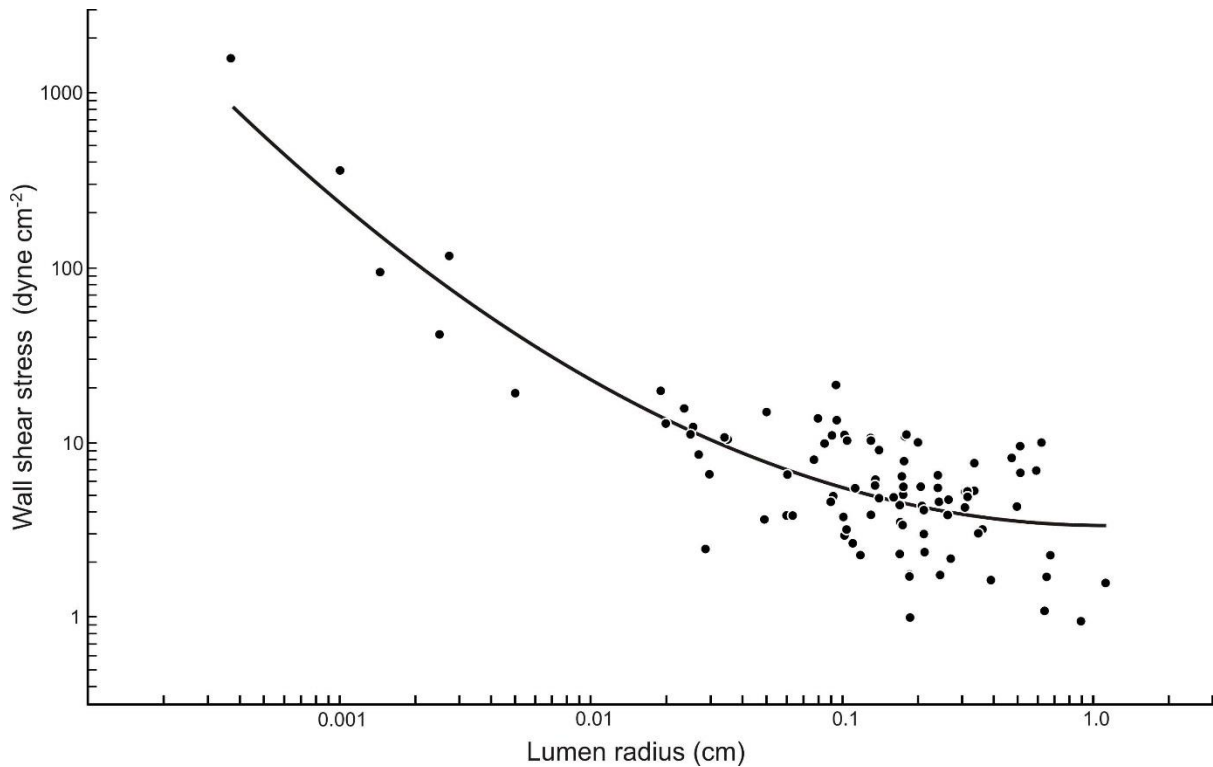
Figure S1. Relationship between log wall shear stress (τ; dyne cm^{-2}) and log systemic arterial lumen radius (r_i; cm) in mammals at rest, calculated from the 'modified' Poiseuille shear stress equation, $\tau = (4\,\dot{Q}\,\eta)/(\pi\,r_i^n)$, where n is the derivative of the equation in Fig. 1 of the main manuscript. The equation for the polynomial mean regression line is: log τ = 0.200 log r_i^2 - 0.017 log r_i + 0.530 (R^2 = 0.70; n = 92).
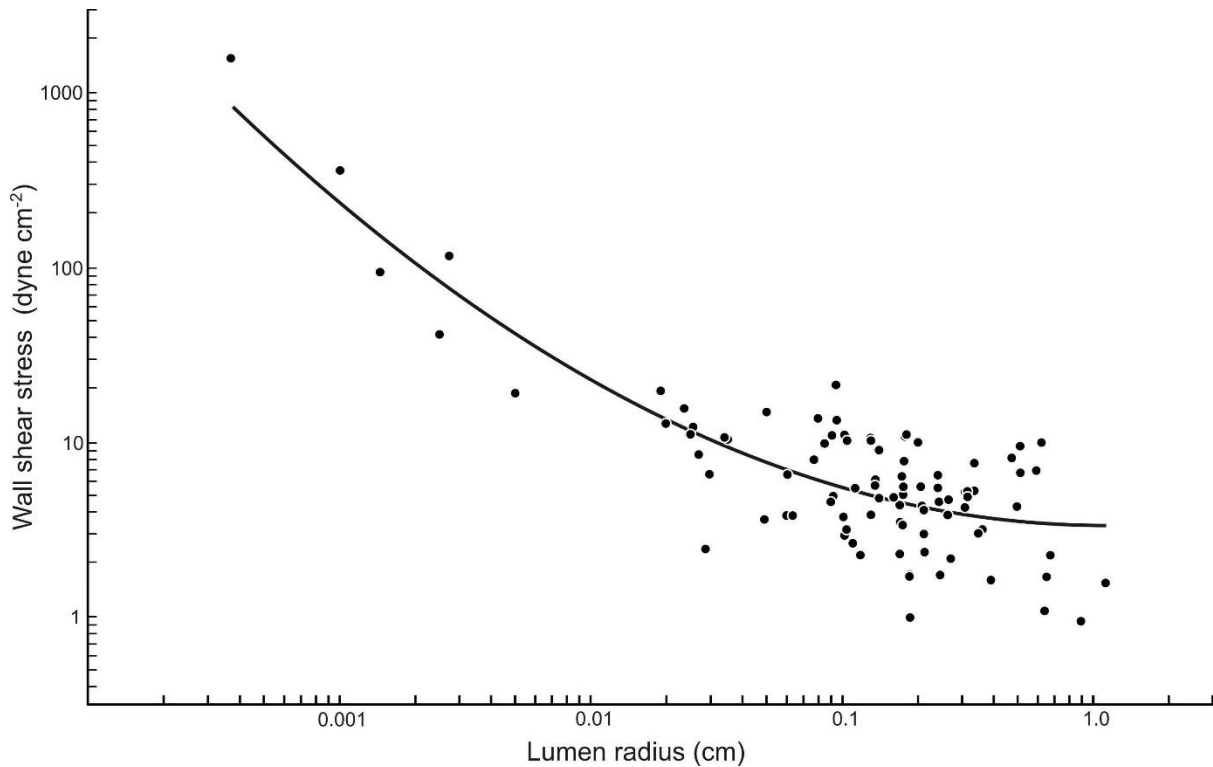
Raw data

Click here to Download Raw Data

Figure S1. Relationship between log wall shear stress (τ; dyne cm^{-2}) and log systemic arterial lumen radius (r_i; cm) in mammals at rest, calculated from the 'modified' Poiseuille shear stress equation, $\tau = (4\,\dot{Q}\,\eta)/(\pi\,r_i^{\,n})$, where *n* is the derivative of the equation in Fig. 1 of the main manuscript. The equation for the polynomial mean regression line is: $\log \tau = 0.200 \log r_i^2 - 0.017 \log r_i + 0.530$ ($R^2 = 0.70$; n = 92).

Table S1

Click here to Download Table S1